Journal of Power Sources 210 (2012) 38–41

Contents lists available at SciVerse ScienceDirect

Journal of Power Sources

journal homepage: www.elsevier.com/locate/jpowsour

Short communication

Elucidating the role of ultrathin Pt film in back-illuminated dye-sensitized solar cells using anodic TiO_2 nanotube arrays

Peng Zhong[a,b], Wenxiu Que[a,b,*], Jin Chen[a,b], X. Hu[c,*]

[a] Electronic Materials Research Laboratory, School of Electronic and Information Engineering, Xi'an Jiaotong University, Xi'an 710049, Shaanxi, People's Republic of China
[b] International Center for Dielectric Research, Xi'an Jiaotong University, Xi'an 710049, Shaanxi, People's Republic of China
[c] School of Materials Science and Engineering, Nanyang Technological University, Nanyang Avenue, Singapore 639798, Singapore

ARTICLE INFO

Article history:
Received 10 December 2011
Received in revised form 31 January 2012
Accepted 23 February 2012
Available online 3 March 2012

Keywords:
Back-illuminated dye-sensitized solar cell
Ultrathin platinum film
Counterelectrode
Transmittance
Catalytic activity

ABSTRACT

We have systematically studied the effects of ultrathin platinum catalytic films in the sub-10 nm regime on the performance of the back-illuminated dye-sensitized solar cells using anodic TiO_2 nanotube arrays. Results indicate that the maximum power conversion efficiency is achieved with a platinum film of 2.48 nm thickness. The charge transfer resistance sharply decreases from 6.39 $\Omega\,cm^{-2}$ (1.24 nm) to 0.24 $\Omega\,cm^{-2}$ (2.48 nm); however, subsequently, it keeps on increasing to 0.76 $\Omega\,cm^{-2}$ (3.72 nm) and 1.36 $\Omega\,cm^{-2}$ (5.58 nm); finally, it re-decreases to 0.25 $\Omega\,cm^{-2}$ (8.06 nm), and remains stable afterwards. The platinum film morphology and particle size on the counterelectrode have been demonstrated to play an important role in catalytic activity in the ultrathin thickness range. This study is meaningful from the aspect of improving the performance of the back-illuminated devices and reducing cost; and meanwhile sheds light on the main factors of influencing catalytic activity in the ultrathin catalytic films.

1. Introduction

Employment of TiO_2 nanotube arrays represents one solution to trap-limited electron diffusion in dye-sensitized solar cells (DSSCs) or hybrid solar cells [1–3]. The back-illuminated structure has recently attracted great attentions to be used for DSSCs based on anodic TiO_2 nanotube arrays directly grown on Ti sheets. This is due to the following reasons: (1) simplicity for large-area growth of highly-ordered and size-adjustable nanotube arrays on Ti substrates; (2) feasible strategy for improving the device stability because iodine in the electrolyte has an excellent ability of absorbing light in the UV range; this prevented otherwise decomposition of the organic dyes in a front-illuminated device; (3) potential for realization of flexible devices. Up to now, a lot of effort has been made globally to bridge the power conversion efficiency (PCE) gap between the back-illuminated DSSCs having anodic nanotube arrays (>∼8%) [4–7] and the front-illuminated devices based on TiO_2 nanoparticles (11%) [8]. For example, Lin and his coworkers [4] improved the device PCE from 4.34% to 7.37% by rational surface treatments; Diau et al. [5] obtained an optimized device PCE as high as 7.6% via fabrication of long TiO_2 nanotube arrays in a short time using a hybrid anodic method. Ye et al. [7] further carried out a combination of techniques to create hierarchical structures in the anodic TiO_2 nanotubes, and they obtained a 7.75% PCE.

The previous studies [4–7] mainly concentrated on increasing the surface areas of the TiO_2 photoanodes to improve the dye loading; however, one important issue related to the device performance was often neglected concerning the counterelectrodes in such back-illuminated DSSCs using anodic TiO_2 nanotubes. The counterelectrode plays an important role in transferring electrons from external circuit back to the redox electrolyte to reduce I_3^- to I^-. Catalyst such as platinum (Pt) is needed to accelerate the reduction, since the transparent conducting oxide film is not catalytic. Due to high cost of Pt as a noble metal, alternative materials such as carbon-based materials have been tried to substitute Pt [9]. However, the DSSCs prepared using those alternative materials for counterelectrodes showed lower PCE than those prepared using Pt; since Pt provides excellent electrocatalytic activity for triiodide reduction. It was suggested that catalytic activity of Pt inside DSSCs is determined by two factors: the electrochemical active areas and the crystallite size of Pt [10]. No significant difference in the performance of the front-illuminated DSSCs was observed while comparing Pt counterelectrodes with thickness of 2 nm and 415 nm [11].

In back-illuminated DSSCs, besides providing electrocatalytic function and electrode conductivity, Pt layer also controls the optical transmission due to its back-illuminated device architecture. Thus, an ultrathin Pt film should be coated onto the transparent conducting electrode, in order to ensure satisfactory light

* Corresponding authors. Tel.: +86 29 82668679; fax: +86 29 82668794.
E-mail addresses: wxque@mail.xjtu.edu.cn (W. Que), asxhu@ntu.edu.sg (X. Hu).

0378-7753/$ – see front matter © 2012 Elsevier B.V. All rights reserved.
doi:10.1016/j.jpowsour.2012.02.094

absorption of the photoanode. However, to the best knowledge of us, there is no reported study into the effect of thickness of the ultrathin Pt layers on the performance of back-illuminated DSSCs using anodic TiO_2 nanotube arrays. On the other hand, further study of Pt catalytic film with the thicknesses in the sub-10 nm regime in DSSCs is warranted, because it is not fully understood, and it is also meaningful from the aspect of economy. In our study, by employing back-illuminated DSSCs having anodized TiO_2 nanotube arrays as the model device, we investigated the multifaceted issues concerning the Pt-coated counterelectrodes in terms of their optical, electrical, electrocatalytic and morphological properties.

2. Experimental

The fabrication of the anodic TiO_2 nanotube arrays was carried out based on modified procedures as described by Wang and Lin [4]. The anodization process used an electrolyte consisting of 294 ml glycol, 6 ml H_2O and 1 g NH_4F; and lasted 3 h under an applied voltage of 60 V. After annealing at 450 °C for 30 min, the nanotube arrays were sensitized with N719 dye at 25 °C for 24 h. The Pt ultrathin films were sputtered onto the FTO substrates by using a DC SPI-Module Sputter Coater. The applied voltage and current were fixed at 1 kV and 6 mA, respectively. As the sputtering time was varied from 0 to 9.5 min, the Pt film thicknesses were estimated to change according to an equation specific for the sputtering machine. The device encapsulation was similar to what was previously reported [4]. The current–voltage (I–V) curves were recorded by a Keithley SMU 2400 Source Measure unit. The fabricated cells were back-illuminated under a solar simulator (Oriel 91192, AM 1.5G); calibrated by a standard silicon solar cell. The area of the fabricated DSSCs was 0.25 cm^2.

The counterelectrode transmittance was measured by UV–vis Microscope (JASCO-570). The sheet resistances ($R_\square$) of the counterelectrodes were obtained by a four-point probe measurement (ST512-SZT-2). The charge transfer resistances (R_{ct}) between the electrolyte and the counterelectrode were obtained from the DSSCs by electrochemical impedance spectroscopy (EIS) under illumination. The magnitude of the alternative signal is 10 mV with frequency range from 10^5 to 10^{-2} Hz. The counterelectrode morphology was characterized by Atomic Force Microscope (AFM) (Veeco Nanoscope). The length of the fabricated TiO_2 nanotube arrays was measured by Scanning Electron Microscope (SEM) (JSM-6700F).

3. Results and discussion

Fig. 1(a) shows the I–V curves of devices prepared using Pt counterelectrodes sputtered for six different durations. They are referred to Pt-1, Pt-2, Pt-3, Pt-4.5, Pt-6.5 and Pt-9.5; corresponding to devices having Pt layers sputtered for 1 min, 2 min, 3 min, 4.5 min, 6.5 min and 9.5 min. The Pt thicknesses are indicated in legend of Fig. 1(a). The inset of Fig. 1(a) illustrates the structure of the back-illuminated DSSC which consists of Pt-coated FTO counterelectrode, liquid electrolyte, and dye-sensitized TiO_2 nanotube arrays on a Ti sheet. The diameter and wall thickness of TiO_2 nanotubes are about 120 nm and 10 nm, respectively. According to the cross-sectional SEM observation (figures not shown), a nanotube length of about 26.9 μm can be fabricated at present conditions. Fig. 1(b) shows the detailed photovoltaic parameters as a function of the Pt sputtering time. The PCE has a sharp increase from 2.44% (1 min) to 4.29% (2 min), a nearly 80% enhancement; with increasing the time, the PCE decreases to 3.32% (3 min), and subsequently, to 2.23% (4.5 min); then the PCE curve shows a platform from 2.23% (4.5 min) to 2.21% (6.5 min); with further increasing the time, the PCE keeps on decreasing to 0.98% (9.5 min). The open-circuit

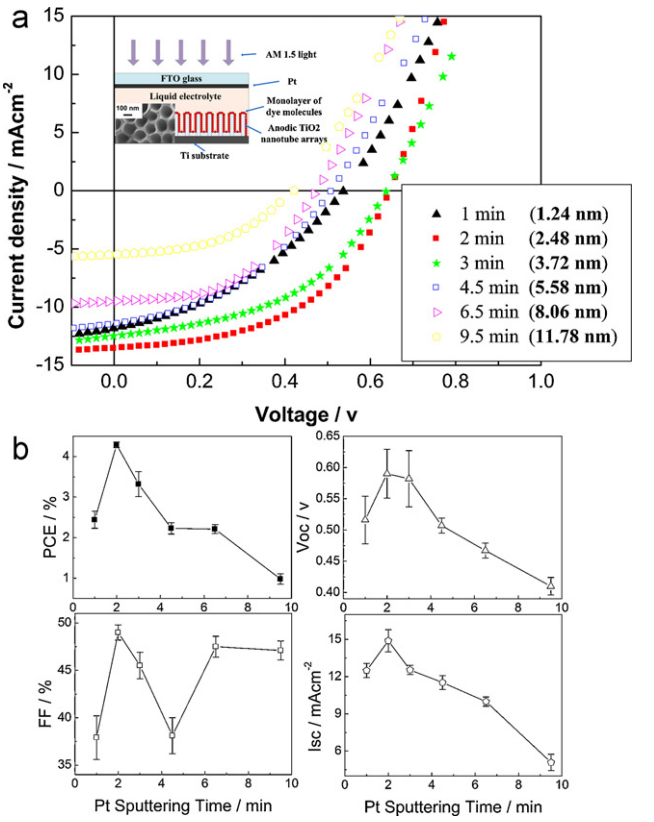

Fig. 1. (a) I–V curves of the DSSCs with different Pt sputtering time. The insert is the schematic of the device structure of the back-illuminated DSSC using anodized TiO_2 nanotube arrays. (b) Detailed photovoltaic parameters (PCE, V_{oc}, FF, I_{sc}) as a function of the Pt sputtering time.

voltage (V_{oc}), the short-circuit current (I_{sc}) and the fill factor (FF) all increase greatly from 1 min to 2 min as the PCE; beyond 2 min, the V_{oc} and I_{sc} continuously deteriorate; however, unlike V_{oc} and I_{sc}, the FF firstly deceases from 2 min to 4.5 min, and then increases from 4.5 min to 6.5 min, until it keeps stable afterwards.

Fig. 2(a) shows the EIS Nyquist plots of the fabricated DSSCs. Based on the equivalent circuit (shown in the top inset of Fig. 2(a)), EIS data can be fitted and gives R_{ct}. The left inset of Fig. 2(a) shows the values of R_{ct} and $R_\square$ as a function of the Pt sputtering time. It can be observed that $R_\square$ with different Pt sputtering time remains stable, which is due to the fact that the Pt films are very thin at present conditions. However, R_{ct} of Pt-2 is much smaller than that of Pt-1 as shown in Fig. 2(a). Because Pt serves as the catalyst for triiodide reduction, the drastic decrease of R_{ct} at 2 min as compared to that at 1 min implies an acceleration of the I_3^- reduction rate. Both $R_\square$ and R_{ct} contribute to the internal series resistance. Since the dye-sensitized TiO_2 nanotube arrays and the Nernst diffusion of I_3^- in the electrolyte were kept unchanged, the variation of internal series resistance can only be attributed to the differences of R_{ct} caused by the Pt layer. It is known that the internal series resistance deteriorates FF of solar cells. As a result, the FF of Pt-2 is much larger than that of Pt-1 as shown in Fig. 1(b). On the other hand, due to much faster I_3^- reduction rate in Pt-2 than that in Pt-1, the electron recombination within the electrolyte could be reduced, which also has an influence toward FF. The exchange current density (j_0) can be achieved across the interface of Pt and electrolyte, and is expressed as [12]:

$$R_{ct} = \frac{RT}{nFj_0} \quad (1)$$

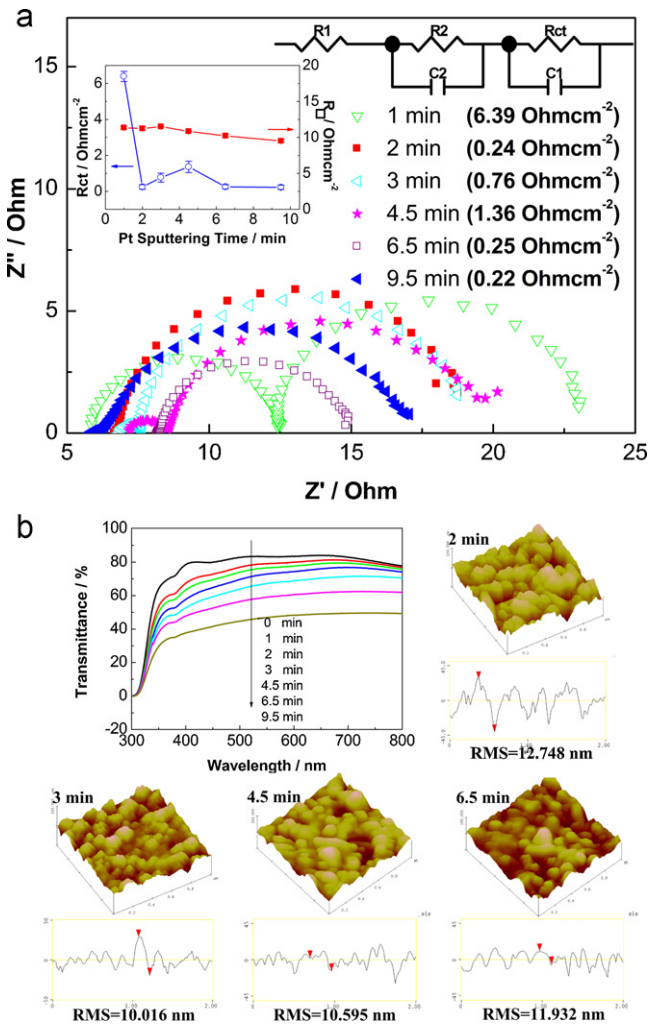

Fig. 2. (a) EIS Nyquist plots of the back-illuminated DSSCs with the Pt sputtering time; the top insert shows the equivalent circuit, where R_1 is a lumped series resistance for the transport resistance of FTO and all resistances out of the cell, R_2 is the recombination resistance between electron and the electrolyte, C_2 is the chemical capacitance, R_{ct} is the charge transfer resistance in the interface between the electrolyte and the Pt film coated on FTO and C_1 is the interfacial capacitance at the counter electrode/electrolyte interface; the left inset shows the resistances ($R_{\square}$, R_{ct}) as a function of the Pt sputtering time. (b) UV–vis spectra, AFM morphology and cross-sectional profiles of the counterelectrodes with different Pt sputtering time.

j_0 of Pt-1 is only 2 mA cm^{-2}, while j_0 of Pt-2 increases sharply to as high as 53 mA cm^{-2}. Theoretically, the largest photocurrent density of DSSCs is about 23 mA cm^{-2}. Therefore, Pt film of 2 min has much better catalytic ability than that of 1 min. A great increase of the I_{sc} can be observed from Pt-1 to Pt-2, as shown in Fig. 1(b). It's interesting to find from Fig. 1(b) that the V_{oc} of Pt-2 is about 0.1 V higher than that of Pt-1. V_{oc} can be calculated from the following equation [13]:

$$V_{oc} = \frac{E_{F,TiO_2} - E_{F,redox}}{q} \quad (2)$$

where E_{F,TiO_2} is the electron Fermi level under illumination, and $E_{F,redox}$ is the redox level of the electrolyte, which can be expressed as follows [14]:

$$E_{F,redox} = \tilde{\mu}_{e,redox} = \mu^0_{redox} + kT \ln\left(\frac{[I_3^-]}{[I^-]}\right) \quad (3)$$

where $\tilde{\mu}_{e,redox}$ is the electron electrochemical potential in the electrolyte. Since Pt-2 has much smaller R_{ct}, i.e. much better catalytic ability for I_3^- reduction, the concentration of accumulated I_3^- on the

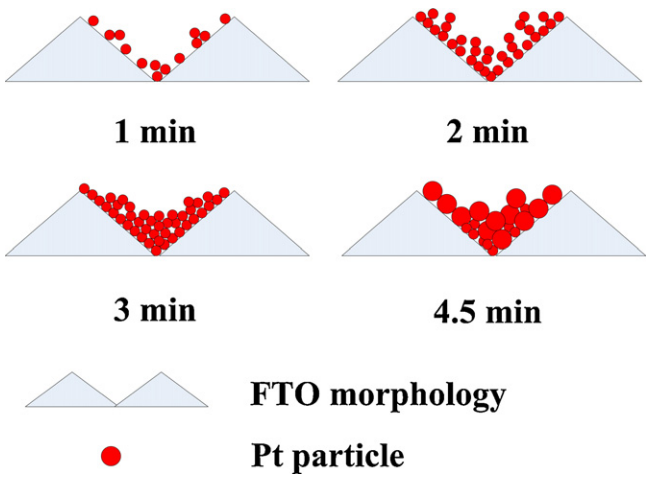

Fig. 3. Schematic of the evolution mechanism of the ultrathin Pt films on the FTO surface with the sputtering time.

counterelectrode made of Pt sputtered for 2 min should be much smaller than that for 1 min. It can be inferred from Eq. (3) that $E_{F,redox}$ would have a negative shift from Pt-1 to Pt-2; which in terms of Eq. (2) results in an obvious increase of V_{oc}, as shown in Fig. 1(b).

The top left part of Fig. 2(b) shows the UV–vis transmittance spectra of the counterelectrodes with different Pt sputtering durations. Although the transmittance decreased with Pt sputtering time, a nearly 80% increase of PCE could be achieved from Pt-1 to Pt-2, indicating that the Pt catalytic ability greatly influenced the device performance in this range. However, the obvious decrease of PCE (23%) from Pt-2 to Pt-3 cannot be simply ascribed to the decrease of transmittance (only 5% at 522 nm of N719 peak absorption). As shown in Fig. 2(b), the Pt film at 2 min has a rougher surface than that at 3 min; giving larger root-mean-square (RMS) roughness. The performance decrease from Pt-2 to Pt-3 should be mainly due to denser Pt film at 3 min i.e. smaller surface area and decreased catalytic ability; which is proven by an increased R_{ct} as shown in Fig. 2(a). Similarly, the continuous deterioration of PCE from Pt-3 to Pt-4.5 should also be mainly caused by the increase of R_{ct} as shown in Fig. 2(a). Although the RMS at 4.5 min is a little bigger than that at 3 min, the Pt particle size at 4.5 min is much larger than that at 3 min, as shown in Fig. 2(b); which would also result in increased R_{ct} i.e. decreased catalytic ability [10,15]. As shown in Fig. 2(a), the R_{ct} above 6.5 min drops back to the level as that of 2 min, indicating that more Pt loading amount compensates for the loss of catalytic ability in the range from 3 min to 4.5 min; which causes the PCE curve platform from 4.5 min to 6.5 min and the PCE decrease at 9.5 min, competing with the light transmittance loss of the counterelectrode. For better understanding the influence of Pt film on catalytic activity, we propose a possible evolution mechanism of Pt ultrathin films on the FTO glass with the sputtering time as illustrated in Fig. 3. It can be observed from Fig. 3 that at 1 min, scattered Pt particles cannot achieve a full coverage on the mountain-like FTO surface, which obviously cannot guarantee satisfactory catalytic activity at this point. With increasing the sputtering time to 2 min, a rough Pt film forms, which supplies enough catalytic areas for triiodide reduction. With further increasing the time to 3 min, Pt particles fill into the FTO valleys to a large extent, and a much denser film forms in this case; although more Pt loading amount exists at 3 min as compared to that at 2 min, the electrochemical active areas are in fact reduced at 3 min, so the Pt catalytic activity was decreased at 3 min as compared to that at 2 min. At 4.5 min, the Pt small particles grow up to much bigger ones in many places, which undoubtedly would further reduce the Pt catalytic activity.

Since the above assumption is well consistent with the AFM and resistance results, we believe that the Pt film morphology and particle size play a significant role in determining the catalytic activity in the ultrathin thickness range; which is very different from what was reported previously [11] in a system with thicker Pt films.

4. Conclusion

In summary, we have demonstrated in this work that by delicately controlling the ultrathin Pt layer, there is much room for enhancement of PCE of back-illuminated DSSCs using anodic TiO_2 nanotube arrays; because this device architecture possesses several advantages, and the recent PCE is approaching the record made by nanoparticle-based cells. The knowledge on the underlying physics and delicate control of the ultrathin Pt layer are important for achieving a more efficient DSSC using anodic TiO_2 nanotube arrays (maybe 10% tomorrow). The present study also gives new insight into the influence of the Pt film thickness on the DSSCs' performance in a small range (1.24–11.78 nm). Besides, this work is of economical significance for both back- and front-illuminated DSSCs, and will be helpful for other types of back-illuminated solar cells [16,17].

Acknowledgements

This work was supported by the Ministry of Science and Technology of China through 863-project under Grant 2009AA03Z218, the Major Program of the National Natural Science Foundation of China under Grant no. 90923012, the Research Fund for the Doctoral Program of Higher Education of China under Grant 200806980023, and the Xi'an Applied Material Innovation Fund Project under grant XA-AM-201006. The authors also thank Mr. Liang Yen Nan for useful comments on the manuscript. Part of the work was carried out at the Nanyang Technological University in Singapore through an international student exchange program.

References

[1] P. Zhong, W. Que, J. Zhang, Q. Jia, W. Wang, Y. Liao, X. Hu, J. Alloys Compd. 509 (2011) 7808–7813.
[2] T.R.B. Foong, Y. Shen, X. Hu, A. Sellinger, Adv. Funct. Mater. 20 (2010) 1390–1396.
[3] P. Zhong, W. Que, X. Hu, Appl. Surf. Sci. 257 (2011) 9872–9878.
[4] J. Wang, Z. Lin, Chem. Mater. 22 (2010) 579–584.
[5] L. Lin, C. Tsai, H. Wu, C. Chen, E. Diau, J. Mater. Chem. 20 (2010) 2753–2758.
[6] B. Lei, J. Liao, R. Zhang, J. Wang, C. Su, D. Kuang, J. Phys. Chem. C 114 (2010) 15228–15233.
[7] M. Ye, X. Xin, C. Lin, Z. Lin, Nano Lett. 11 (2011) 3214–3220.
[8] Q. Yu, Y. Wang, Z. Yi, N. Zu, J. Zhang, M. Zhang, P. Wang, ACS Nano 4 (2010) 6032–6038.
[9] T. Murakami, S. Ito, Q. Wang, M. Nazeeruddin, T. Bessho, I. Cesar, P. Liska, R. Humphry-Baker, P. Comte, P. Pechy, M. Gratzel, J. Electrochem. Soc. 153 (2006) A2255–A2261.
[10] C. Zhou, Y. Yang, J. Zhang, S. Xu, S. Wu, H. Hu, B. Chen, Q. Tai, Z. Sun, X. Zhao, Electrochim. Acta 54 (2009) 5320–5325.
[11] X. Fang, T. Ma, G. Guan, M. Akiyama, T. Kida, E. Abe, J. Electroanal. Chem. 570 (2004) 257–263.
[12] N. Papageorgiou, W.F. Maier, M. Gratzel, J. Electrochem. Soc. 144 (1997) 876–884.
[13] Q. Wang, S. Ito, M. Grätzel, F. Fabregat-Santiago, I. Mora-Sero, J. Bisquert, T. Bessho, H. Imai, J. Phys. Chem. B 110 (2006) 25210–25221.
[14] A. Nozik, R. Memming, J. Phys. Chem. 100 (1996) 13061–13078.
[15] H. Feng, J. Libera, P. Stair, J. Miller, J. Elam, ACS Catal. 1 (2011) 665–673.
[16] Z. Fan, H. Razavi, J. Do, A. Moriwaki, O. Ergen, Y. Chueh, P. Leu, J. Ho, T. Takahashi, L. Reichertz, S. Neale, K. Yu, M. Wu, J.W. Ager, A. Javey, Nat. Mater. 8 (2009) 648–653.
[17] R. Tao, J. Wu, H. Xue, X. Song, X. Pan, X. Fang, X. Fang, S. Dai, J. Power Sources 195 (2010) 2989–2995.